Chemical Engineering Journal 430 (2022) 132619

Contents lists available at ScienceDirect

Chemical Engineering Journal

journal homepage: www.elsevier.com/locate/cej

Direct electrochemistry and enzyme-involved photo-electrocatalysis of oxygen reduction for the electrode on the basis of titanium dioxide-graphene oxide nano-complex with laccase accommodation

Shu Wei Zhang, Mi Zhang, Fang Wang, Han Zeng *

Xinjiang key laboratory of energy storage and photoelectrocatalytic materials, Chemistry and Chemical Engineering Academy, XinJiang Normal University, XinJiang Uyghur autonomous region, Urumuqi 830054, PR China

ARTICLE INFO

Keywords:
Titanium dioxide
Graphene oxide
Laccase
Photo-electrocatalysis
Oxygen electro-reduction

ABSTRACT

Nano-complex consisting of Titanium dioxide and graphene oxide via covalent bonding was proposed to be Laccase immobilization matrix through collaborative effect of chemical tethering and adjacent complexation between TiO_2 and Laccase molecule. Geometrical feature, structural characteristics and physio-chemical properties of nano-composite with Laccase entrapment were systematically characterized and evaluated. Influences of mutual interactions between element of nano-complex and incorporated protein molecule on kinetics of electro-catalysis and efficiency of photo-electrocatalysis for oxygen reduction of Laccase based electrode were quantitatively analyzed. Results from measurements indicated mutual interactions dominated by adjoining ligation would lead to irregular arrangement of protein molecules on the surface of enzyme carrier and decrease the orderliness of nano-complex with Laccase anchoring with improved hydrophilicity. The combination of Laccase with P25 in nano-complex via the static quenching would enhance the utilization efficiency of external illumination with the crippled band gap (Eg) in the indirect mode (~1.43 eV for nano-composite with Lac integration). Such combination would alter the route of charge transferring which meant the redox site in TiO_2 would play the role of primary electron acceptor and T_1 site in coordination with TiO_2 of integrated Laccase could perform the duty of intra-molecular electron mediator (apparent heterogeneous electron shuttle rate: 2.6×10^{-3} s^{-1}). Electro-catalytic performance on oxygen reduction for Laccase based electrode was limited by the step of substrate diffusion (in the form of free state and entrapment into nano-complex: 2.9×10^{-4} and 1.8×10^{-6} s^{-1}, respectively). As-prepared Lac case based electrode displayed favorable sensing performance to its substrate-dissolved oxygen: high affinity (K_M: 46.4 μmol•L^{-1}), moderate detection limit (0.34 μmol•L^{-1}) and enhanced sensitivity (0.021 μA•L•μmol^{-1}).

1. Introduction

Photo-sensitive electrode is the essential element for conversion and storage device of solar energy. Explorations concerning about the improvement in the preparation process and composition of photo-sensitive electrode to exalt its efficiency are considered to be beneficial to boost the advance in the usage of clean energy. Relevant investigations have been the research focus for last decades [1]. TiO_2 as the most popular semi-conductor materials is considered to be the suitable candidate to prepare the novel photo-sensitive electrode with high efficiency for its unique advantages such as: controllable conformation, superior photo-sensitivity, low cost, favorable physical stability and predominant bio-compatibility. Low electrical conductivity and narrow window of irradiation absorption could restrain the wide application of TiO_2 as the building block of photo-electrochemical instrument [2]. TiO_2 alone as matrix to accommodate bio-macromolecules could lead to the loss in aboriginal activity of bio-catalysis resulting from the negative influence of mutual interactions between TiO_2 and bio-macromolecules. Furthermore, the combination of bio-macromolecules with TiO_2 would cripple the efficiency of photoelectric conversion to great extent for the overlapping of non-conductive bio-molecule backbone. Unfortunately, related investigations about these issues have not been performed in depth as for [1,2]. Graphene oxide (GO) as typical carbon based nano-material is well-known for its desirable thermal

* Corresponding author.
E-mail address: zenghan1289@163.com (H. Zeng).

https://doi.org/10.1016/j.cej.2021.132619
Received 24 July 2021; Received in revised form 19 September 2021; Accepted 20 September 2021
Available online 24 September 2021

conductivity, high specific surface area, good mechanical strength and excellent electrical conductivity. Edge of GO could be modified by many functional groups such as –OH, $-NH_2$, –SH and –COOH. Such modification could facilitate the firm linkage of bio-macromolecules (e.g., DNA, nucleic acid and redox protein) with GO or GO based nano-complex. Disadvantages of GO as the carrier of bio-molecules are the low mass loading of bio-macromolecule and relatively inferior activity in bio-catalysis from the conglomeration of bio-molecules at the fringe of GO via hydrogen bonding and electrostatic attraction.

The combination of GO with TiO_2 would prevent from possible agglomeration of TiO_2 to maintain its high specific surface area and more chemical active sites on the surface of nano-composite would be achieved to allow high loading capacity of bio-macromolecules (i.e., redox enzyme molecule) [3–6]. Such integration could enhance the efficiency in charge shuttle of nano-complex. Such combination would improve the conductivity of TiO_2 alone as the element of photo-sensitive electrode. It would also prohibit from the combination of electron with cavity in TiO_2 to improve the photo-electrochemical activity [5]. Most researches have focused on the electro-chemical behaviors and evaluation on the performance of photo-electrocatalysis for the as-prepared electrodes on the basis of GO based nano-composite with bio-macromolecules integration to the best of our knowledge [7–13]. Metal elements in nano-composite and hetero-atoms of components within nano-complex would impose considerable effect on configuration, constellation and charge transferring mechanism of bio-macromolecules integration into nano-composite via multiple interactions such as hydrogen bond effect, electro-static interaction, chemical coupling and abutting coordination as described in early reports. Unfortunately most of past efforts did not provide exact and clear explanation the influence of mutual interactions between element of nano-composite (e.g., metal element in nano-complex) on electro-chemical behavior and electro-catalytic efficiency of bio-macromolecules accommodation into nano-complex so far [8,11–12].

On the basis of previous discussions and conceptions, TiO_2 was covalently coupled up with GO to act as Laccase (Lac) carrier via the synergistic effect of covalent bonding and abutting ligation. Previous research efforts did barely involve the role for elements of nano-complex (i.e., Titanium dioxide and GO as enzyme carrier in this paper) with protein attachment in the enzymatic electro-catalysis [4,10–11]. The impacts of mutual interactions between components of nano-composite and enzyme molecules such as covalent coupling and adjoining ligation on the steps of enzyme-involved electro-catalysis are the main objective of the investigation in this submission. Such influences resulting from these interactions on the route of charge transferring and relevant mechanism of electro-catalysis on oxygen reduction reaction (ORR) has been elucidated in detail. A variety of characterization and measurement including spectrometry, electron microscopy and electrochemical means were proposed to elucidate the variation in configuration, surface chemical feature, electro-chemical properties and the detail of enzymatic electro-catalysis. Such comprehensive investigation has been seldom implemented in comparison to previous research works until now [4, 7 and 12]. Quantitative analysis in procedures involved in the Lac-induced electrocatalysis was made to determine the rate determining step of the whole catalysis. Such endeavors would promote the deep understanding of essence in physiological activities of organisms to design and manufacture the bio-mimetic instrument with high performance.

2. Experiment

2.1. Reagents and apparatus

N-hydroxysuccinimide (NHS) and Chitosan (CTS, degree of deacetylation: ≥90%, molecular weight: ~250000 g•mol-1) were acquired from Aladdin chemical reagent Co., Ltd in Shang-Hai of China. Lac from Fungal Myrothecium verrucaria (Molecular mass: ~68000 g•mol-1, specific activity to 2, 2′-azino-bis-(3-ethylbenzothiazoline-6-sulphonic acid) diammonium salt (ABTS): 0.5 U•mg-1), industrial Titanium dioxide (P25), GO and N-(3-Dimethylaminopropyl)-N'-ethylcarbodiimide hydrochloride (EDC) were supplied by Sigma chemical reagent Co, Ltd, USA. Other conventional chemicals with analytical purity in the experiments were provided by Tian-Jin Zhi-Yuan Chemical reagents Co, Ltd (China) and sinopharm Co., Ltd in China, respectively. 79–1 type magnetic stirring apparatus was acquired from Jinyi instrument and technology Co., Ltd, Jiang-Su in China. 2 K15 type refrigerated ultra centrifuge for separation of nano-composite with Hb attachment from discrete phase was bought from Sigma Company in Germany. The electrolyte in electro-chemical measurement was 0.2 M phosphate buffer solution (PBS) with pH regulation which was prepared with similar method described elsewhere [14–15]. Nitrogen gas with high purity was obtained from Kangdi Special Gas Co., Ltd, China.

TG16WS desktop high speed centrifuge was obtained from Jingli Centrifuge Co., Ltd, Beijing in China. BRUKER D2 model diffractometer was manufactured by BRUKER Co, Ltd in Germany. JSM-7610FPlus scanning electron microscope with accelerating voltage of 0.5 ~ 30.0 kV and variable resolutions: 1.0 (15 kV) and 1.3 nm (1.0 kV) was supported by Japanese electrical Co., Ltd in Japan (JEO). TENSOR-27 type Fourier transformation infrared spectrometer was afforded by BRUKER Company, Germany (KBr pellet). Z2000 type atomic absorption spectrometer equipped with graphite furnace atomic absorption spectrophometer (main frame: single beam flame, testing range of wavelength: 190 ~ 900 nm) was provided by HITACHI Company in Japan. UV-3600 type ultraviolet–visible spectrometer was bought from Shimadzu Corporation in Japan (optical length: 1 cm).Chirascan spectropolarimeter outfitted with 150 W Xe lamp as illuminant and air cooling accessory (thickness of quartz color plate: 1.0 cm) was offered by Applied Photophysics Company in UK. Cary Eclipse type spectrofluorometer was produced by Varian Company in USA. Glassy carbon electrode (GCE, diameter: 3 mm) as basal electrode, reference one: Ag/AgCl in saturated KCl aqueous solution and auxiliary one-platinum coil were furnished by Aida Hengsheng industrial and commercial Co, Ltd in Tian-Jin of China. All potentials in the submission are relative to normal hydrogen electrode (NHE) without extra tagging. Pre-treatment of basal electrode and reckoning of active surface areas of GCE over-coated by nano-complex alone and nano-composite with Lac attachment were elucidated in detail early [14–15]. Zahner Zennium electro-chemical platform and CHI-660E electro-chemical working station were secured from Kronach Company in Germany and CHI Inc, Chen-Hua Co, Ltd in Shang-Hai of China, respectively. Indium tin oxide (ITO) glassy panels were supported by Zhuhai Kaiwei photoelectro-technological Co., Ltd in China. CHF-XM500 500 W Xe lamp as light source in photoelectro-catalytic experiment was obtained from Perfectlight Technology Company in Bei-jing of China.

2.2. Preparation procedure and characterization of basal electrode capped by thin film of P25-GO nano-complex with Lac entrapment

Titanium dioxide-GO nano-complex could be secured through conventional hydrothermal method as introduced elsewhere [16]. As-prepared nano-composite was added into PBS and the mixture was incubated under ultra-sonic dispersion for 15 min to prepare evenly distributed discrete phase. EDC and NHS (mass ratio of both elements: 2:1) were pipette into previous dispersed phase to activate surface-tailored carboxylic groups on the interface of GO. Subsequently aliquot of dry Lac powder was plunged into well-proportioned discrete phase under magnetic stirring for 2 h. The mixture was incubated in refrigerator at 4 °C overnight. Nano-complex with Lac was centrifugally separated from the viscous mixture under the rotating rate at 8000 round•mol-1 and supernatant was removed from the system. As-prepared slimy fluid was denoted to be Lac/P25-GO and 15.0 μL nano-complex with Lac accommodation was dripped onto the surface of supporting electrode. Lac based electrode was prepared via traditional

drop-casting method as previous illustration [17] and it was designated to be Lac/P25-GO-CTS/GC. Schematic illustration in composition and preparation procedure of this Lac based electrode was presented in Fig. 1.

Specific capacity of Lac into P25-GO nano-complex could be figured out in compliance with the same means: graphite furnace atomic absorption spectrometry (GFAAS) demonstrated elsewhere [18]. Mass of Lac immobilization into enzyme carrier could be deduced from the change in copper concentration of bulk solution with dissolved Lac before and after redox enzyme integration into matrix. Geometric idiosyncrasy of nano-complex with Lac entrapment could be characterized by scanning electron microscopy (SEM). Preparation procedure of SEM samples was similar to that elucidated early [17]. Features of chemical micro-environment were explored by X-ray diffraction (XRD), Fourier transformation infrared spectroscopy (FTIR), ultra-violet and visible spectroscopy (UV–Vis) and emission fluorescence spectrometry (FRS). XRD spectra were recorded under such experimental parameters as: Cu-Kα as radiation source (testing wavelength λ: 0.154 nm), tube voltage at 30.0 kV, tube current of 10.0 mA and diffraction angle ranging from 10 to 70. Manipulation of UV–Vis measurements was similar to the procedure illustrated previously [19]. Samples of FTIR spectra could be secured via compression of the mixture made up of dry powder for testing target and KBr into tablet and further desiccation. Operational parameters of FRS measurements were listed as follows: excitation wave-length of 280 nm, slit width at 5 nm and window of wave-length scanning: 300 ~ 500 nm. Physicochemical properties of nano-composite with Lac attachment were investigated by circular dichroism (CD), electrochemical impedance spectroscopy (EIS) as well as cyclic voltammetry (CV). EIS spectra were registered under such operational parameters as: frequency ranging from 0.1 to 105 Hz, open circuit voltage of 410 mV and disturbance voltage at 5.0 mV. Steady CV curves were recorded at the potential sweeping rate of 100 mV•s-1, nitrogen atmosphere and the potential range from −1.0 to 1.0 V. Determination in mechanical stability of nano-composite with Lac incorporation was carried out in accordance with the same working flow mentioned early [20].

2.3. Electrochemical behavior and photo-electrocatalysis on oxygen reduction of Lac based electrode on the basis of P25-GO nano-complex

All electro-chemical experiments at steady status operating under local pressure and room temperature (26.5 ± 0.6 °C) without additional denotation were conducted in conventional electrolytic cell consisting of three electrodes in deaerated or oxygen-saturated PBS. Lac/P25-GO-CTS/GC was used to be working electrode as the research target in this article. CV, chronoamperometry (CA) and differential pulse voltammetry (DPV) were proposed to study and evaluate the direct electrochemistry and catalytic performance on electro-reduction of O_2 for as-prepared Lac based electrode. Steady CV curves were acquired within the potential window from −1.0 to 1.0 V and scanning rates under modulation. DPV curves were registered under potential sweeping rate at 100.0 mV•s^{-1}, potential ranging from −1.0 to 1.0 V and step potential at 5 mV. CA experiment was implemented via tracking of steady current response to addition of dissolved oxygen molecules with time lapse for Lac/P25-GO-CTS/GC in magnetic stirring PBS under constant applied potential of −0.4 V according to the previous description [21]. Efficiency of photo-electrocatalysis on oxygen reduction for ITO panel modified by nano-complex with Lac integration was evaluated with current–time curve under external illumination (500 W Xe lamp as light source equipped with UV cutoff filter at 420 nm). Lac based ITO electrode was prepared via similar drop-casting procedure depicted previously. i-t curves were recorded under the switching between “on” and “off” status at the time interval of 100s.

3. Results and discussion

3.1. Characterization and investigation in geometric feature, structural characteristics and physicochemical properties of P25-GO nano-complex with Lac attachment

Specific accommodation amount of Lac into P25-GO nano-composite could be estimated to be 119.7 mg•g^{-1}. This value is apparently superior to those ones of Lac immobilization into GO (43.4 mg•g^{-1}) and Lac in connection with PO (68.7 mg•g^{-1}). Such result indicated that the combination of P25 and GO would aggrandize the loading capacity of

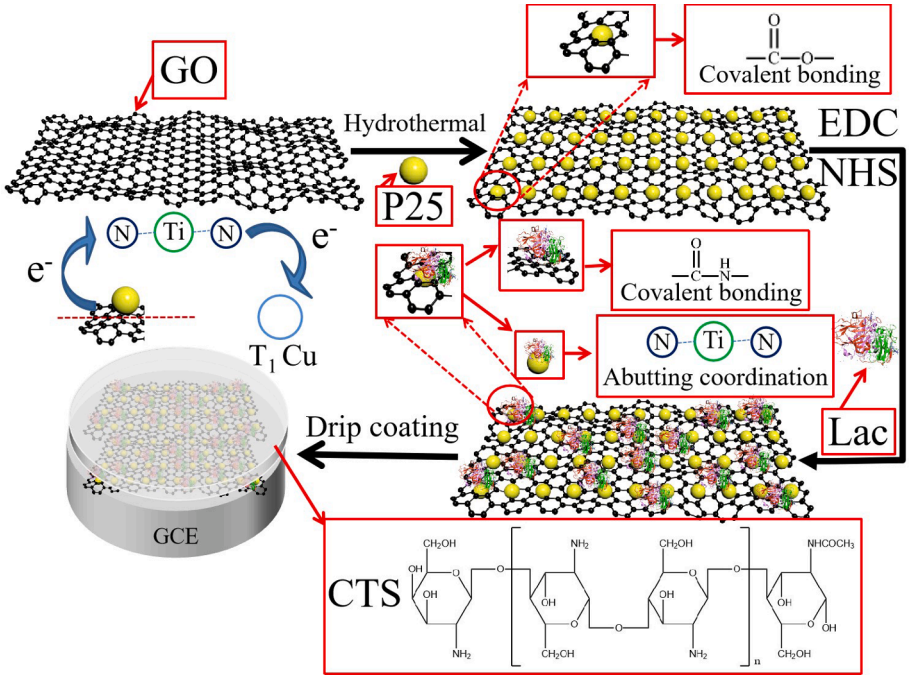

Fig. 1. Schematic illustration in the composition and preparation process of Lac/P25-GO-CTS/GC.

enzyme molecules into as-prepared complex via collaborative effect of covalent bonding and neighboring ligation mentioned previously. Catalytic activities on 2, 6-dimethoxyl phenol (DMP) oxidation characterized by UV–Vis as the demonstration in former research effort [18] for the following cases: free Lac, Lac attachment on GO, P25 with Lac tethering and P25-GO with Lac integration could be determined to be 14.6, 10.9, 4.7 and 6.8 U•mg^{-1}. Such result indicated that the synergy of abutting ligation and chemical coupling would alleviate the negative effect of direct osculation between P25 and Lac on inherent efficiency of enzyme-involved catalysis. All these attested the nano-complex via the combination of P25 with GO as the enzyme supporter could not only exalt the loading amount of enzyme into the matrix but also facilitate to exert its native function on the enzyme-induced catalysis to some extent.

SEM images of P25, P25-GO nano-complex alone and nano-composite with Lac anchoring were shown in Fig. 2. Granular clusters from aggregation of small P25 particles with quasi-spherical shape could be identified from Fig. 2A. Such morphology of P25 should be put down to hydrogen bond interaction between hydroxyl groups on the surface of P25 particles. Such conglomeration would debase the surface active area and it would lead to the shrinkage in the utilization of external irradiation. Geometric feature of P25-GO was distinct from both systems of P25 and GO demonstrated elsewhere [22]. Coinstantaneous appearance of huge P25 clots and GO sheets could be identified from Fig. 2B. Moreover, relatively smaller curds of P25 on the interface of GO could be detected. The latter should be in connection with mutual interactions between GO and P25 including hydrogen bond interaction, chemical coupling and adjoining complexation. It should be noted that most clots of P25 conglomeration could be discerned on the edge and pleat-like structure of GO. Such result resulted from the abundance of hydrophilic groups on these sites (i.e. hydroxyl group and carboxylic group) within GO. This feature could provide the opportunity of chemical bonding between P25 and GO and P25 would be moored on these binding sites. Floccule-like appearance of P25-GO nano-complex with Lac tethering and essential disappearance in inherent morphology of elements in nano-composite (i.e. GO and P25) could be recognized in Fig. 2C. A plenty of smaller and unformed agglomerates could be found in the microscopic image of nano-composite with Lac accommodation. Such morphological feature should be attributed to the random distribution of Lac onto the surface of nano-complex via the combination of Lac with elements of nano-complex (i.e. GO and P25). Broad scattering of Lac molecules on the surface of nano-complex instead of congregation onto specific spots within the carrier of protein is consistent with the high accommodation mass of P25-GO nano-complex in comparison to those of element alone within nano-composite.

XRD spectra of industrial Titanium dioxide: P25 and P25-GO nano-complex were exhibited in Fig. 3. Main diffraction peaks located at 25.3°, 36.9°, 37.7°, 47.9°, 53.8°, 54.9°, 62.6° and 68.6° could be discerned in the spectrum of P25. These signals should be in connection with crystalline surfaces of anatase TiO_2 as illustration in the standard spectrum (JCPDS, No.21–1272): (101), (103), (004), (200), (105), (211), (204) and (116) with their corresponding interlayer spacing: 0.352, 0.243, 0.238, 0.190, 0.170, 0.167, 0.148 and 0.137 nm. Similar featuring peaks of anatase Titanium dioxide with slight positive shift in peak location could be identified in the XRD spectrum of P25-GO nano-composite. Furthermore, no extra diffraction peak could be detected in

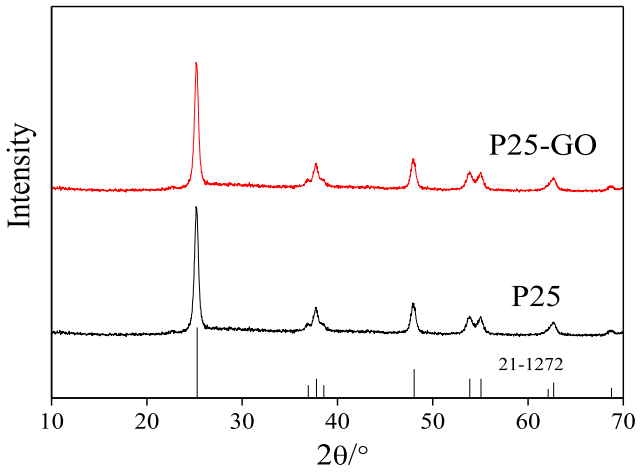

Fig. 3. XRD spectra of P25 as well as P25-GO nano-composite (the standard spectrum of anatase TiO_2: JCPDS, No.12–2172 is included in Fig. 3).

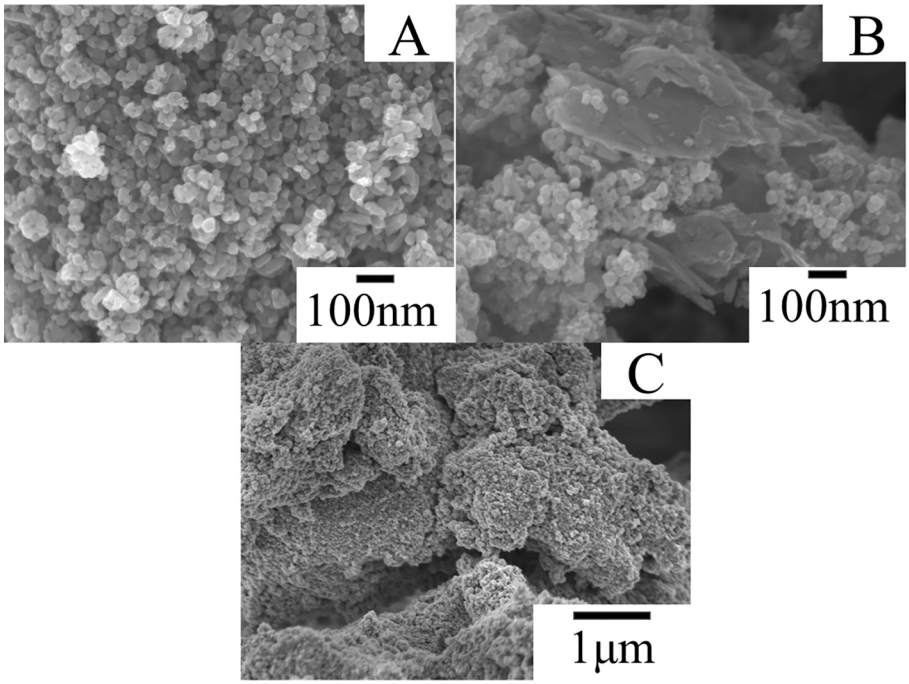

Fig. 2. SEM images of Titanium dioxide (A), P25-GO nano-composite (B) and nano-complex with Lac tethering (C).

the XRD spectrum of nano-complex. Original ones for GO and pristine graphite (the sharp peak at 9.8° and the halo peak at 26.3° for crystalline surface: (002)) [23] would be covered up by that of P25. All these suggested that mutual interaction between ZIF-8 and P25 was relatively weak and the crystalline feature of nano-complex could be dominated by that of P25. Such conclusion was consistent with the analysis in microscopic images. Narrow interlayer spacing indicated Lac molecules (dimension: 5.5 ~ 6.5 nm) could not intercalated into the gap between layers within P25-GO nano-composite and Lac molecules could only be attached onto the surface of nano-complex.

FTIR spectra of P25, P25-GO nano-complex alone, free Lac and nano-composite with Lac tethering were displayed in Fig. 4. Idiosyncratic bands of Titanium dioxide (e.g. –OH stretching vibration peak at 3307 cm^{-1}, distinct peaks at 447.4 and 491.5 cm^{-1} for Ti-O) could be detected in the FTIR spectrum of P25. Characteristic absorption peak of GO (i.e. the featuring peak at 1635 cm^{-1} of –C = C in huge π conjugation system within GO) [23] could be found in the spectrum of P25-GO nano-complex. Only one diagnostic peak at 464.0 cm^{-1} for Ti-O stretching vibration could be discerned in the spectrum of nano-complex. Such result indicated the appearance in distinct peak of Ti-O should be imputed to the adjoining ligation of Ti and O atom in ester bond and covalent coupling of P25 with GO. This assumption could be consolidated by the appearance of some unsight bands in the spectrum of nano-composite. It meant the disappearance of –OH after the formation of ester bond band and the appearance of featuring band for the ester bond (stretching vibration peak of C-O-C at 1236 cm^{-1} [16] could be detected in the spectrum of nano-complex. It should be noticed that the band of –C = O in ester could be over-lapped by that of –C = C- within GO and was not recognized from the spectrum of nano-complex alone. The existence of characteristic peak at 1728 cm^{-1} for C = O in carboxylic group implied the abundance of free –COOH which could be used to tether Lac molecules via the formation of amido bond. Some remarkable variations in locations of featuring bands for elements of nano-composite with Lac integration could be detected in the spectrum of P25-GO with Lac anchoring. Further negative shift in the band of Ti-O (at ~ 440.0 cm^{-1}) suggested the impact of adjacent coordination between Ti and hetero-atoms within amido bond or surface amino acid residues of Lac incorporation into nano-complex on bond energy of Ti-O [19]. Violet shift in wavelength for C = O in amido I band of Lac (1708 cm^{-1}) accommodation into nano-complex in comparison to that of native Lac (1652 cm^{-1}) could be identified in the spectrum of nano-complex with Lac attachment. Simple coupling of Lac with nano-material via amido bond could lead to red shift in the location of amido I band to some extent as described previously [22]. For example, featuring peak of C = O within amido I for Lac anchoring into GO via covalent tethering could be recognized at ~ 1640.0 cm^{-1} (data not shown). The violet shift in the location of amido I band for Lac should be ascribed to the interference of complexation between metal elements and hetero-atoms in nano-composite with enzyme detainment. All these results indicated the collaborative effect of covalent coupling and abutting coordination on micro-chemical environment of nano-complex with Lac entrapment would be dominated by the adjoining ligation between TiO_2 and amino acid residuals of Lac [17].

UV–Vis spectra of native Lac, P25, P25-GO nano-composite and nano-complex with Lac were illustrated in Fig. 5. No obvious absorption band at higher than 250 nm could be detected in the spectrum of free enzyme molecule for the deep embedding of multi-copper sites in the inner structure of Lac and copper site in the reduced state in the absence of strong oxidant. Only one main absorption peak at ~258 nm and another side peak at 315 nm could be found in the spectrum of P25 and it could be put down to the inner electron transportation transition from the valence band of O 2p to the conductive band of Ti 3d [13]. Remarkable attenuation in the strength of the former band and slight red-shift in the latter one (approximate 4 nm to 319 nm) after GO adulteration into P25 could be detected in the spectrum of P25-GO nano-complex. Compared with the absorption edge of native P25, that of P25-GO nano-complex displayed distinguished red shift. The prominent red shift suggested that the band gap of P25 with GO coupling could be narrowed. Such results should be imputed to the connection of TiO_2 with GO via covalent coupling and competitive ligation between Ti and O in ester bond introduced previously. The apparent shrinkage in the peak strength at 258 nm should be imputed to the mutual interactions between GO and P25 and overlapping of this signal with the characteristic peak of GO at 250 nm. The featuring band of GO originated from π-π electron transition in carbon backbone. Similar phenomenon with relatively higher magnitude could be identified in the spectrum of nano-composite with Lac accommodation. It indicated that this nano-complex with enzyme entrapment would be excited by external illumination to produce collaborative effect [13]. Such effect could facilitate the charge transferring of photo-induced electron from conduction band of P25 to unoccupied orbital of GO with shortened band gap. It also suggested the minor impact from the interaction between Lac and P25 on photo-electrical activity. This deduction could be supported by the calculation on the values of band gap (Eg) in the indirect mode for as-prepared P25 (2.58 eV), P25-GO (1.72 eV) and nano-composite with Lac anchoring (1.43 eV). Such estimation could be conducted with the similar method introduced elsewhere [23].

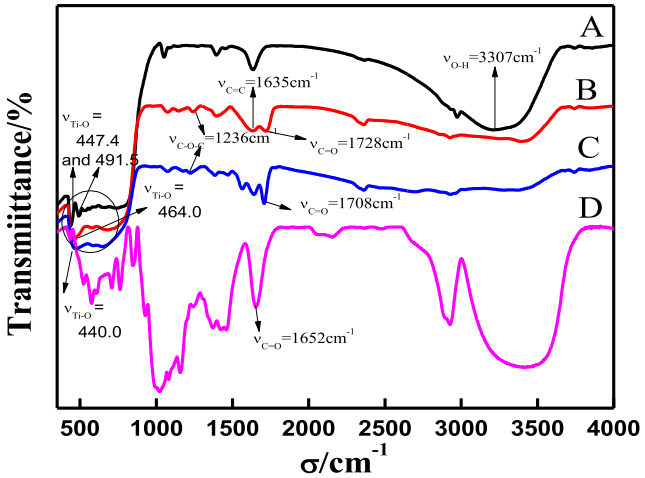

Fig.4

Fig. 4. FTIR spectra of Titanium dioxide (A), P25-GO nano-complex alone (B), P25-GO nano-composite with Lac coupling (C) and native Lac (D).

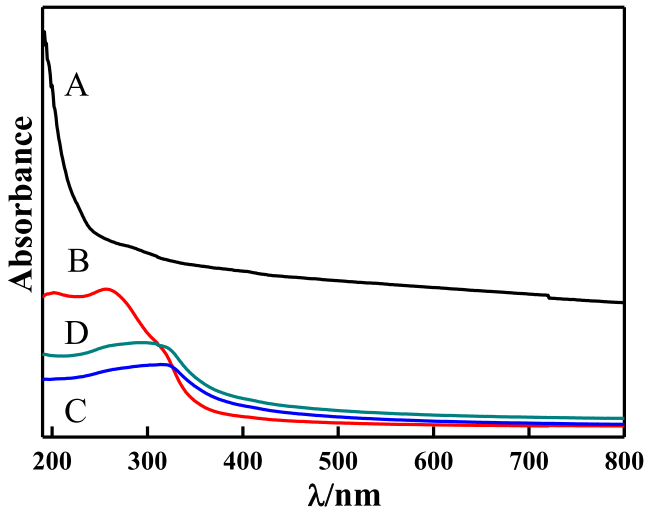

Fig. 5. UV–Vis spectra of free Lac (A), Titanium dioxide (B), P25-GO nano-complex alone (C) and nano-composite with Lac integration (D).

CD spectra of native Lac, P25-GO nano-complex and nano-composite with Lac tethering were unfolded in Fig. 6. Three sharp and negative absorption peaks located at 204, 210 and 213 nm could be observed in the spectrum of free protein. Existence of these peaks should be related to the secondary structures of redox protein molecule such as α-helix and β-pleated sheet (i.e. hydrophobic structures) [22]. Distinct and strong negative absorption peaks at 204, 210, 213 and 217 nm could be detected in the spectrum of nano-complex alone and it revealed the presence of hydrophobic structure units: gigantic π electron conjugated system and the complex of Ti with O atom in ester bond. Remarkable difference could be identified in the case of nano-composite with Lac accommodation in comparison to previous both ones. It meant that only negative bands near 204 nm of native Lac was utterly disappeared and two consecutive and negative absorption peaks at 213 and 216 nm could be detected. The former one with crippled intensity could be distinguished and it should be ascribed to the introduction of hydrophilic groups via the formation of amido bond between Lac and the GO. The latter one should be in connection with the competitive coordination of P25 with surface amino acid residues of Lac. All these convinced the ascension in disorder after Lac integration into nano-complex and improved hydrophlicity for the introduction of abundant hydrophilic groups. Such conclusion was in compliance with the result of SEM experiments and analysis in FTIR spectra.

FRS spectra of a series of mixtures consisting of free Lac at constant concentration and P25 under content modulation and corresponding Stern-Volmer plot were demonstrated in Fig. 7A and Fig. 7B. Amino acids with fluorescence emission in Lac are comprised of phenylalanine (Phe), tryptophan (Trp) and tyrosine (Tyr). Usually fluorescence emission of Trp was proposed to investigate the change in configuration of Lac molecule for low fluorescence quantum yield of Phe and easy extinction in fluorescence emission of Tyr [24]. Two main emission bands at 310 and 335 nm could be recognized in the spectrum of native Lac and these peaks should be attributed to diagnostic signals for the existence of Trp and Tyr. Disappearance of emission peak at 335 nm with the increase in content of P25 revealed the exposure of amino acid residuals within inner structure of Lac in the presence of competitive complexation between P25 and Lac. At the same time, the intensity of Trp featuring band would be attenuated and the location of this band would make a violet-shift with the ascension in content of P25. Such result should be put down to the combination of P25 with Trp via adjoining ligation between Ti and N atom in Trp structure mentioned previously. Distinguished emission peaks at 365, 381 and 424 nm could be detected in Fig. 7A after the addition of TiO_2 into solution with dissolved Lac. The latter ones should be ascribed to the idiosyncratic peaks of anatase TiO_2 itself. The former one should be in connection with the

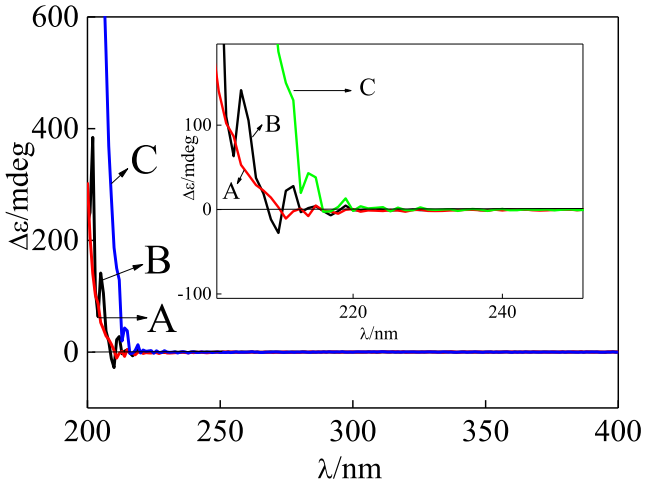

Fig. 6. CD spectra of aboriginal Lac (A), P25-GO nano-complex alone (B) as well as nano-composite with Lac immobilization (C).

interaction of P25 with Trp to produce complex. It should be stressed that interaction between GO and Lac could be considered to be minor for the almost identical spectrum of mixture made up of Lac and GO in comparison to that of free Lac. According to the analysis in linear-fitting Stern-Volmer plot shown in Fig. 7B, the combination procedure of P25 with Trp in Lac should be classified into a classical static quenching mode for the normalized fluorescence quenching constant (K_q, 4.7×10^{11} L•(mol•s)$^{-1}$ could be derived via the similar means elucidated elsewhere [25]) much higher than the threshold of K_q for most quenching reagents to bio-macromolecules (2.0×10^{10} L•(mol•s)$^{-1}$). It meant that this combination would give birth to interim species with unique spectroscopic and other physicochemical properties. Moreover, number of binding sites for the combination process and binding constant K could be figured out to be 1 and 2.16×10^{10} L•mol^{-1} in compliance with the same method described elsewhere [25]. All these indicated that the interaction between Lac and P25 was rather strong. However this relatively strong interaction would not distort the inherent configuration of Lac molecule essentially. Such assumption could be supported by the fact that Lac molecules immobilization into nano-complex could catalyze the oxidation of DMP efficiently as described early (nano-composite alone would not achieve the same effect at the same maximum absorption wavelength). Original catalytic efficiency of native Lac could be kept to some extent as previous expectation.

Fig. 8A illustrated EIS spectra of bare GCE, GCE capped by P25, basal electrode with P25-GO nano-composite modification and supporting electrode over-coated by P25-GO nano-complex with Lac tethering in static and nitrogen-bubbling PBS containing electrochemical probing species. Relevant CVs of four electrodes in the same electrolyte were exhibited in Fig. 8B. Common feature of EIS spectra for these as-prepared electrodes could be identified that the shape of impedance curves could be considered to be composed of semicircle arc portion and linear segment. Diameter of the former is proportional to the resistance in charge transportation [26]. The slight reduction in resistance of electron shuttle for GCE with P25 modification and the remarkable one for basal electrode capped by P25-GO nano-complex alone could be observed in Fig. 8A. Such results should be imputed to the successful combination of P25 with conductive GO. This conclusion could be considered to be consonant with the analysis in UV–Vis spectra as discussed previously. Correspondingly, current response of electro-chemical probing species for these cases would be enhanced respectively. Such results was in related to the augment in active surface area and electric conductivity for the introduction of GO which displayed favorable capability of charge convection [27]. Apparent rise in resistance of charge transferring could be detected after Lac integration into nano-complex. It should be noted that the value of electron conveyance resistance for the electrode on the basis of nano-complex with Lac immobilization was near to that of GCE with P25 modification and was relatively lower than that of bare supporting electrode. Corresponding shrinkage in current response of electro-active species could be monitored for this system. No other electro-chemical signal could be recognized within the potential sweeping window from the CV of Lac based electrode in PBS with electro-chemical probing reagent. Elevation in resistance of electron transporation and reduction in redox peak current of electro-chemical probing species should be imputed to the existence of insulative protein backbone and reduction in active surface area. It also suggested that the novel electro-active species resulting from the combination of Lac with P25 described previously would contribute to the improvement in the ability of charge shuttle in comparison to that of Lac immobilization into GO-CTS composite (data not presented). Complete disappearance in the redox peaks of electro-chemical probing species could be detected in the former case. The combination of $K_3Fe(CN)_6/K_4Fe(CN)_6$ with surface amino acid residues of Lac integration into GO would lead to the formation of complex without any capability of charge transferring.

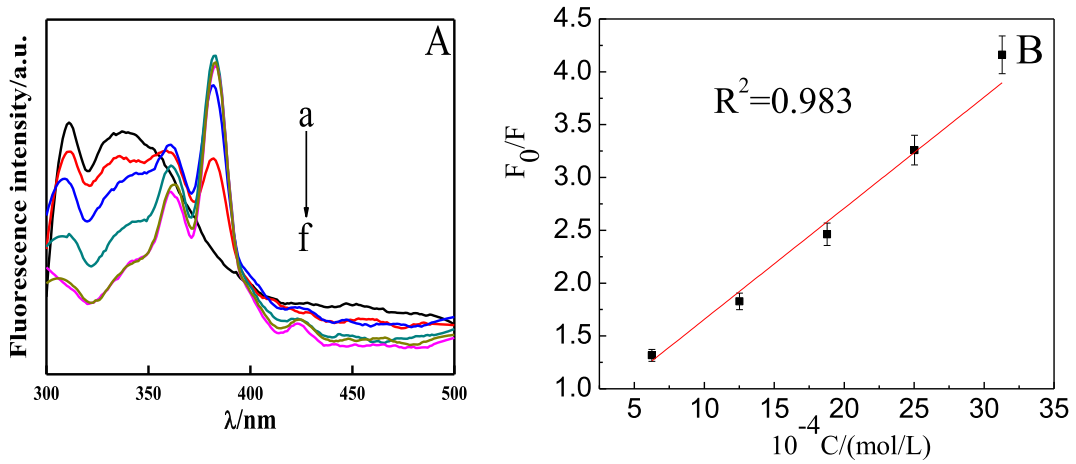

Fig. 7. FRS spectra for a series of mixtures made up of dissolved free Lac at constant concentration level of 0.25 mg•mL^{-1} and P25 with contents in regulation (a-g indicating: 0, 0.05, 0.1, 0.15, 0.2, 0.25 , 0.3 mg•mL^{-1}) (A) and corresponding Stern-Volmer plot for mutual interactions between P25 and aboriginal Lac molecule, data could be derived from the average value of five replicate measurements (B).

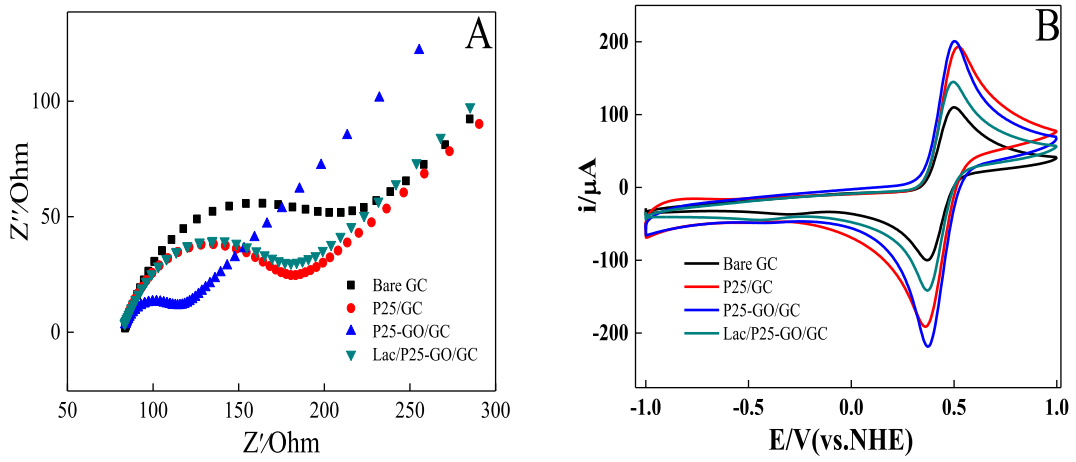

Fig. 8. EIS spectra (A) and CVs recorded under the potential scanning rate of 100.0 mV•s^{-1} (B) of bare GCE, basal electrode over-coated by P25, supporting electrode capped with P25-GO nano-complex and Lac/P25-GO-CTS/GC in deaerated aqueous solution with 2.5 mM $K_3Fe(CN)_6$ + 2.5 mM $K_4Fe(CN)_6$ + 0.1 M KCl.

3.2. Direct electrochemistry, electro-catalytic performance on ORR and photo-electrocatalysis on ORR of electrode based on P25-GO nano-composite with Lac accommodation

CV curves of P25-GO nano-complex alone based electrode and electrode on the basis of nano-composite with Lac immobilization in oxygen-free and O_2 bubbling PBS recorded at moderate rate of potential sweeping were displayed in Fig. 9, respectively. Twin conjugated and asymmetric peaks (anodic/cathodic currents ratio: $i_{p,a}/i_{p,c}$ at ~ 1.85) with mean peak potential of 331 mV could be detected in i-E curve of GCE with P25-GO nano-complex modification. Large potential gap (356 mV) and anisomerous shape of CV for nano-composite based electrode indicated unfavorable reversibility and inferior dynamics of charge convection of redox reaction occurred on the surface of this electrode. Such electro-chemical signal should be put down to the redox process of electro-active groups within P25-GO complex. The electro-chemical feature of this composite could be considered to be dominated by TiO_2 in comparison to that of similar nano-composite made up of GO and organic dye without electro-activity as demonstrated elsewhere [22]. Similar asymmetric redox bands with relatively bigger $i_{p,a}/i_{p,c}$: 2.08 and slightly narrowed potential gap (306 mV) could be observed in the CV of Lac/P25-GO-CTS/GC. Both electrodes also demonstrated apparent catalytic effect on oxygen reduction with almost identical onset potential of electro-catalysis in comparison to those of

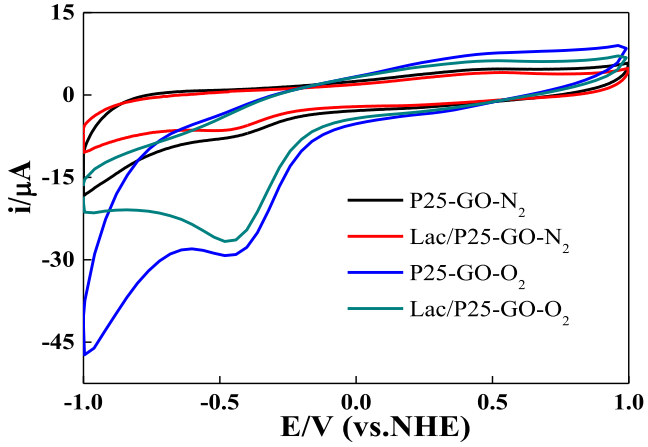

Fig. 9. CVs of static GCE with P25-GO nano-complex modification and Lac/P25-GO-CTS/GC in oxygen-free and O_2 saturated PBS (pH = 4.4) registered at the potential sweeping velocity of 100.0 mV•s^{-1}.

TiO_2 based composite consisting of TiO_2 and organic molecule as well as GO based complex made up of GO and organic dye [22]. It suggested that the complex of TiO_2 with surface amino acid residues would display superior affinity to dissolved oxygen molecules in comparsion to native cofactor within Lac. It is well-known that the onset potential of ORR could be recognized near the formal potential of T_1 site in Lac (500 ~ 800 mV [28], if the direct electron transferring between cofactor in Lac and conductive interface of supporter could be accomplished). High ovpotential for ORR in this case implied that the enzyme-induced electro-catalysis on oxygen reduction would be suppressed by the complexation of P25 with Lac. It should be noticed the onset potential of ORR for Lac based electrode was close to mean potential of redox bands for P25-GO nano-complex based electrode. Catalytic current of ORR for Lac based electrode would be crippled prominently in relation to that of electrode based on P25-GO nano-complex alone for the elevation in active energy of oxygen molecule transformation into reduced product. All these implied that the electro-catalysis on ORR was dominated by redox group of P25 and TiO_2 in coordination with surface groups of Lac could play the role of intra-molecular electron relay. Such deduction was consonant with the analysis in FRS spectra mentioned early. Furthermore, common trait of both systems could be identified and it meant the appearance of sharp reduction peak at ~ -465 mV for the electro-reduction of entrapped oxygen molecules into nano-complex [19] with and without Lac anchoring.

CVs of static Lac/P25-GO-CTS/GC in PBS purged by nitrogen gas registered under potential sweeping different rates and relevant linear-fitting plots of oxidation and reduction peaks currents for P25 in coordination with surface residues of Lac against scanning rates were unfolded in Fig. 10A and its inset. The potential gaps between oxidation peak and reduction one for the primary redox site within nano-complex with Lac accommodation referred early were almost identical with the ascension in sweeping rate as shown in Fig. 10A. The redox peaks currents of the dominant electro-active site within nano-complex with Lac entrapment would augment linearly with the increase of scanning velocity within the testing window of the potential sweeping rate as demonstrated in inset of Fig. 10A. All these convinced that the redox procedure of Lac based electrode should be classified into a typical surface-confined mode of electro-chemical reaction [29]. Additionally side oxidation peak could be monitored under moderate rates of potential sweeping. Such phenomenon indicated that the electro-chemical reaction occurred on the surface of Lac based electrode could be regarded as the assembly of a series of consecutive redox processes. TiO_2 in ligation with surface groups of Lac with superior electro-activity and T_1 site within Lac as intra-molecular electron mediator would be involved in this complicated redox procedure of Lac/P25-GO-CTS/GC. Dependence plot of potential gap between oxidation peak and reduction one under rapid potential sweeping on logarithm of potential scanning velocity was shown in Fig. 10B. Potential difference would be enlarged linearly with the ascension in logarithm of the potential scanning rate as illustrated in Fig. 10B. Apparent heterogeneous electron transferring rate (k_s) and electrons involved in the redox procedure of Lac based electrode would be calculated to be 2.6×10^{-3} s^{-1} and 2.0 with the Laviron equation introduced elsewhere [22,28,30], respectively. The latter was distinguished from usual value: 1 of electrical-wired T_1 site within Lac immobilization into nano-materials described elsewhere [31–32]. This result was consistent with the feature of Ti based redox process between Ti^{4+} and Ti^{2+}. It meant that redox site of P25 could act as the primary electron acceptor and could dominate the consecutive redox processes. Furthermore, the diffusion co-efficient of attached O_2 molecules into nano-complex could be derived from the slope in linear-fitting plot of reduction peak currents at the potential negative than −0.5 V against the square root of potential scanning rates as depicted previouly [15]. This parameter (at the magnitude of 10^{-7} $cm^2 \bullet s^{-1}$) was much lower than the dissolved oxygen molecules in aqueous system (1.7×10^{-5} $cm^2 \bullet s^{-1}$).

DPVs for static Lac/P25-GO-CTS/GC in oxygen-free PBS without any external electron relay registered under moderate rate of potential scanning and modulated pulse heights in positive and negative sweeping were illustrated in Fig. 11A and Fig. 11B, respectively. A series of consecutive and broad oxidation bands consisting of main peak at relatively negative potential and side one at positive potential (i.e. near 0.5 V) could be observed at low pulse heights in Fig. 11A. The location of the first oxidation band would shift negatively and the side peak would be diminishable with the elevation in pulse height in the positive sweeping as shown in Fig. 11A. Similar result could be identified in the negative scanning as depicted in Fig. 11B. Moreover, extra reduction band at ~ -0.5 V in the negative scanning could be identified at any pulse height. The former indicated the existence of distinct redox sites with variable electro-activity [19] consisting of the primary one in P25-GO nano-complex with superior performance in electron transferring and the second one of T_1 site in Lac as intra-molecular electron relay with inferior electro-activity. The latter revealed that oxygen molecules could be entrapped into nano-composite and could be reduced at stable and negative potential. Such conclusions were in accordance with the

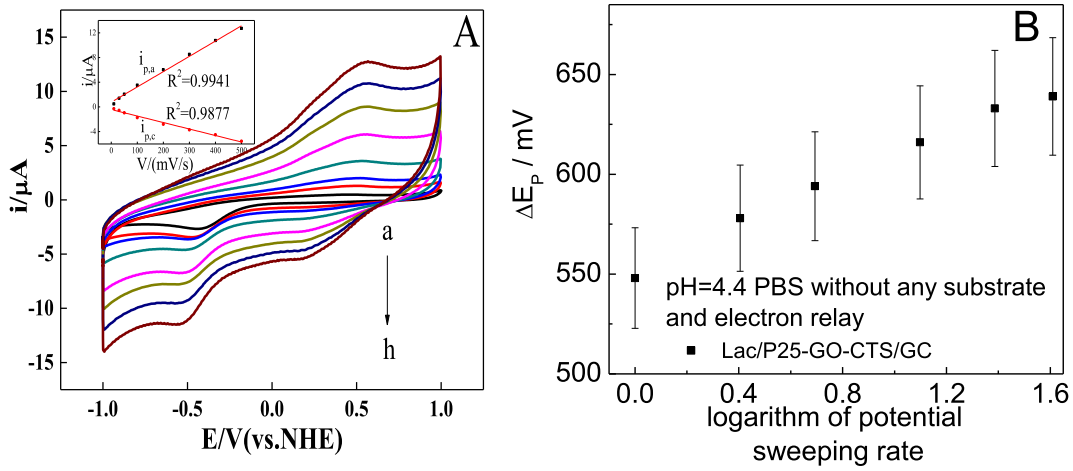

Fig. 10. CVs of quiescent GCE over-coated by thin film of P25-GO nano-composite with Lac incorporation in slightly acidic PBS (pH = 4.4) without any external electron mediator recorded at modulated potential sweeping rates (a ~ h indicating: 10, 30, 50, 100, 200, 300, 400, 500 $mV \bullet s^{-1}$) (A), its inset: linear-fitting relationship plots of redox peak currents versus potential scanning velocity of Lac/P25-GO-CTS/GC; dependence plot of redox peak potential difference on logarithm of potential sweeping velocity for static Lac/P25-GO-CTS/GC in deaerated PBS(pH = 4.4), data were figured out from the average value of five repeated tests (B).

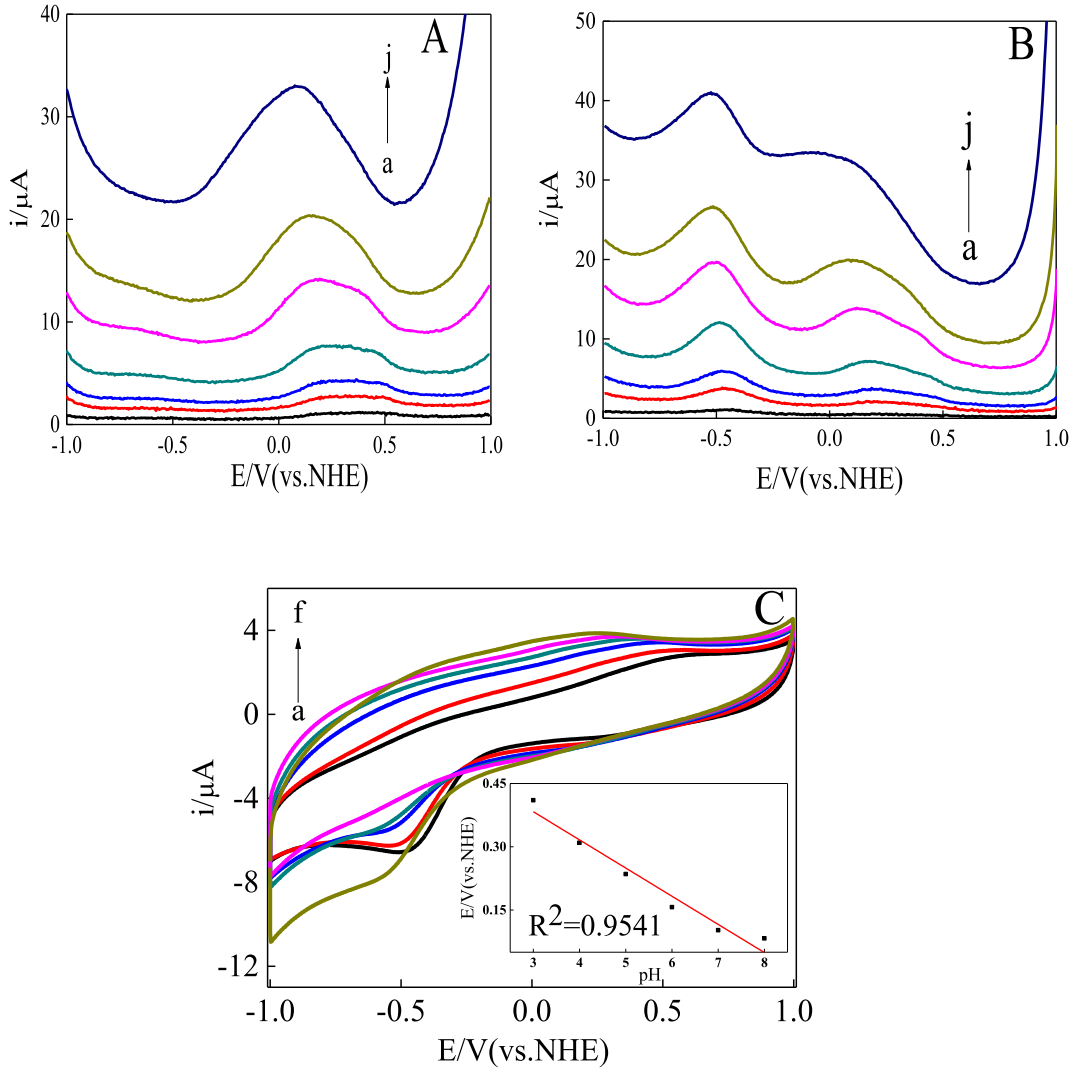

Fig. 11. DPVs of static Lac/P25-GO-CTS/GC in N_2 bubbling PBS (pH = 4.4) without any external charge relay registered under different pulse heights (a ~ g for pulse heights at 10, 30, 50, 100, 200, 300 and 500 mV) and the potential sweeping rate at 100.0 mV•s^{-1}, in the positive (A) and negative (B) potential scanning; CVs of immobile Lac/P25-GO-CTS/GC in N_2 stream purging PBS with pH manipulation registered under the potential sweeping velocity of 100.0 mV•s^{-1} (a ~ f: pH value at 3.0, 4.0, 5.0, 6.0, 7.0 and 8.0) (C), its inset: linear-fitting plot of mean value of redox peak potentials for Lac based electrode versus pH of PBS throughout the experiments.

previous analysis in CV curve of Lac based electrode in the same electrolyte.

CVs of static electrode on the basis of P25-GO nano-composite with Lac anchoring in oxygen-free PBS under pH regulation recorded under moderate rate of potential scanning and corresponding linear-fitting plot of mean peak potential for redox peaks of Lac/P25-GO-CTS/GC against pH value of PBS were depicted in Fig. 11C and its inset. Naturally peak potentials of redox peaks for Lac based electrode would shift negatively with the elevation in pH value of electrolyte according to the Nernst equation. Favorable linear relationship between mean peak potential for Lac based electrode and pH value of buffer solution could be retained within the testing pH range. Slope of linear-fitting plot could be extrapolated to be −66 mV/pH and the redox process should be imputed to an electro-chemical reaction with 2 electrons and 2 protons involved. Considering the absence of H^+ in the electron shuttle process of redox site within TiO_2 and the number of H^+ (i.e. n = 1) involvement in the redox process of GO based electrode [22], one H^+ could be regarded as participation in the redox process for the complex of TiO_2 in coordination with surface residues of Lac.

A series of steady CV curves for Lac/P25-GO-CTS/GC in slightly acidic and electron relay-free PBS with O_2 concentration regulation recorded at moderate rate of potential sweeping were ushered in Fig. 12A. Dependence plot of reduction peak current on the consistency of dissolved oxygen molecule was also depicted in inset of Fig. 12A. Decrease in oxidation current and concurrent enhancement in reduction one could be discerned with the introduction of from Fig. 12A. Catalytic reduction current would be augmented and the onset potential of catalysis near formal potential for redox group of P25-GO nano-complex would be kept invariable with the elevation in concentration of O_2 in electrolyte. It was obvious that good linear relationship between reduction peak current and content of substrate could be maintained within the testing range of dissolved oxygen molecule. Such result convinced that the combination of Lac with P25 would debase the catalytic function of native cofactor within Lac on ORR with increased active energy of oxygen reduction. It also indicated that as-prepared electrode on the basis of nano-composite with Lac integration was sensitive to the appearance of dissolved oxygen molecules. It should be noticed that related parameters (K_M: 44.1 μmol•L^{-1} and turn-over frequency for ORR: 8.9 × 10^{-3} s^{-1}) of electro-catalysis on ORR derived from Lineweaver-Burk plot as demonstrated elsewhere [31] (data from CV curves in inset of Fig. 12A) for Lac based electrode could be considered to be similar to those ones from CA experiment (see later

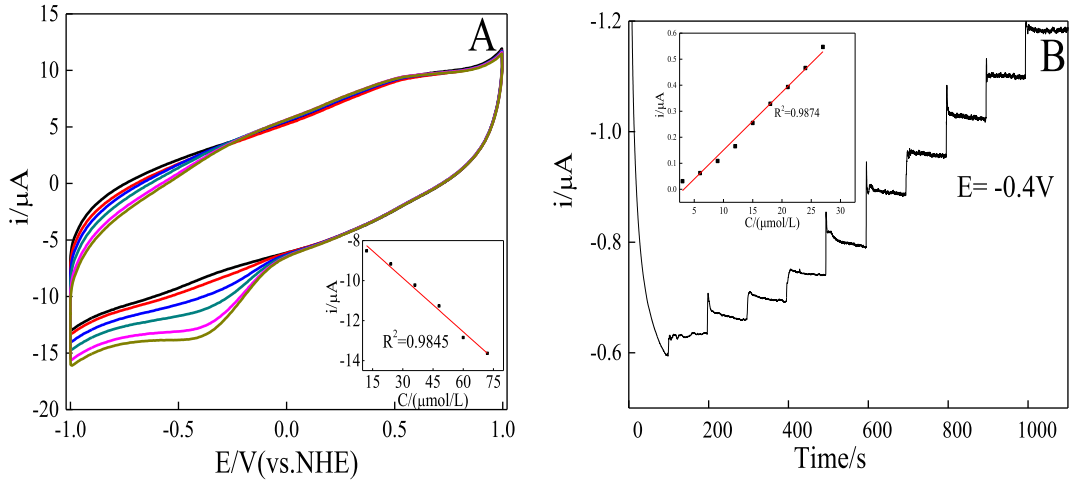

Fig. 12. CVs of static Lac based electrode in a series of PBS at pH = 4.4 with regulated consistencies of dissolved O_2 (from inner to outer curves for concentrations of substrate: 12, 24, 36, 48, 60 and 72 μmol•L^{-1}) in the absence of external electron relay, potential scanning rate: 100.0 mV•s^{-1} , inset graph: linear-fitting plot of steady catalytic current at ~ -0.4 V for Lac based electrode against the concentration of dissolved substrate (A), CA curve of Lac/P25-GO-CTS/GC in magnetic stirring PBS (pH = 4.4) with variable substrate contents at different time intervals recorded at moderate and stable applied potential in the absence of external charge relay (B), its inset: dependence plot of steady catalytic current response on ORR for Lac based electrode on consistency of dissolved oxygen molecules.

statement).

CA curve of Lac/P25-GO-CTS/GC in electron mediator-free PBS with modulated oxygen contents at different time intervals recorded at constant applied potential was demonstrated in Fig. 12B. Inset of Fig. 12B ushered the linear-fitting plot of steady current response for electro-reduction of dissolved oxygen molecules versus consistency of substrate. Result from Fig. 12B manifested that Lac based electrode in this submission displayed swift electro-chemical response to the dissolved oxygen molecules and showed favorable sensitivity to the change in the consistency of dissolved substrate. Oblique shape in so-called "step region" of current–time curve suggested that the dynamics of Lac-induced electro-catalysis could be dictated by the procedure of mass transportation for oxygen in bulk solution or in nano-complex layer on the surface of basal electrode. This assumption was validated by the

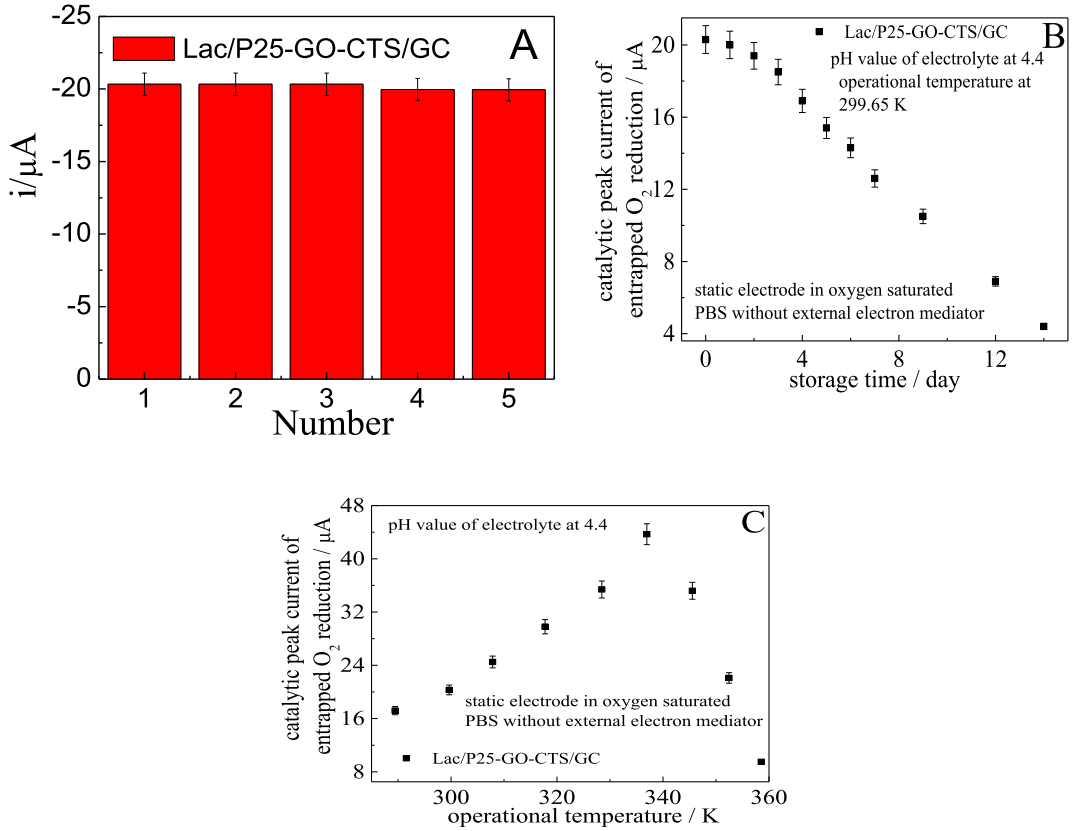

Fig. 13. Reproducibility (A), long-term usability (B) and operational temperature dependence (C) in electro-catalytic function on ORR for Lac/P25-GO-CTS/GC in charge mediator-free PBS saturated by O_2 determined by CV under the same experimental parameters as shown in Fig. 9, data in Fig. 13 could be considered to be the average value of five replicate determinations.

comparison in the values between normalized rate constant of substrate diffusion (whether in the form of free state or in the form of entrapment into nano-composite, normalized rate of mass transferring could be figured out to be 2.9×10^{-4} and 1.8×10^{-8} s^{-1} according to the method described previously [15,33–34]) and that of heterogeneous charge transportation illustrated early. Excellent linear relationship between steady reduction current and the substrate concentration could be kept within the testing concentration window of substrate from inset of Fig. 12B. Improved sensitivity (0.021 μA•L•μmol^{-1}), superior affinity (Michaelis constant-K_M: 46.4 μmol•L^{-1}) and moderate detection limit (0.34 μmol•L^{-1}) in comparison to that of similar system depicted early [19] indicated that the adjacent coordination of P25 with surface groups of Lac would not hinder the substrate binding capability seriously. Furthermore, turn-over frequency of entrapped oxygen molecules for Lac based electrode could be estimated to be 9.4×10^{-3} s^{-1} with the similar means introduced elsewhere [33] (amount of electrical-wired electro-catalyst: 1.3×10^{-10} mol could be calculated from the mean integration area of redox peaks in CV recorded at specific sweeping rate for Lac based electrode as shown in Fig. 10A). Finally normalized rate constant of oxygen molecules attachment on nano-complex could be worked out to be 5.5s^{-1} with the definition elucidated elsewhere [19]. On the basis of quantitative analysis in kinetics of procedures involved in the electro-catalysis, key step in restraining the efficiency of ORR for Lac-based electrode should be imputed to the process of oxygen transportation from stock solution to the surface of conductive matrix or diffusion in nano-composite layer.

Repeatability (A), long-term stability (B) and thermal endurance (C) in electro-catalysis of dissolved oxygen reduction for Lac/P25-GO-CTS/GC were measured with CV under the same operational parameters as shown in Fig. 9. Relevant results were illustrated in Fig. 13. It was evident from Fig. 13A that the difference in catalytic peak current at ~ -0.465 V for ORR of entrapped oxygen molecules was neglectable. Mean value of catalytic peak current for Lac-induced ORR was ~20.3 μA and the RSD in this parameter of five as-prepared Lac based electrodes in the same batch was ~1.1%. This result convinced the gratifying reproducibility in catalytic efficiency on ORR for Lac/P25-GO-CTS/GC could be achieved in this manuscript. Result from Fig. 13B revealed that the catalytic function on ORR would be crippled with the protraction of storage span because of the natural attenuation in catalytic activity of as-prepared composite with Lac anchoring. Similar dependence plot of catalytic performance on storage time could be identified for P25 based electrode (data not provided). It suggested that the catalytic function on ORR was dominated by TiO_2 in nano-composite with Lac incorporation. Dependence plot of catalytic efficiency on ORR for Lac based electrode on experimental temperature as shown in Fig. 13C indicated the bell shape could be recognized and maximum in catalytic effect could be pinned down at 63.8℃. Catalytic performance on ORR would be attenuated sharply when the operational temperature was higher than the optimal one. It should be ascribed to the denaturalization under high heat and acceleration in the formation of complex made up of P25 and amino acid residues on the surface of Lac. FRS experiments implied that the signal intensity for the presence of complex would be enhanced with the increase in the operational temperature (data not provided). UV–Vis experiment also convinced that Lac molecules integration into P25-GO nano-complex would lose most catalytic activity under high temperature. It also manifested that the attachment of Lac on the surface of nano-composite should be classified into typical chemical adsorption [35–36]. Furthermore, investigation on relationship between catalytic peak current of Lac-induced ORR and pH value of buffer solution revealed that catalytic function on ORR for Lac based electrode was almost invariable with the alteration in pH value of electrolyte. Such phenomenon implied that the catalysis on ORR could be dictated by P25 instead of tri-nuclear cluster in Lac (i.e., oxygen binding sites). Extra electro-chemical experiment supported this deduction. It meant the catalytic performance on ORR for P25-GO based electrode could be kept stable under pH value of PBS modulation (data not shown).

The relationship curve of photo-electrocatalytic current versus irradiation span for ITO electrode on the basis of P25-GO nano-complex with Lac immobilization in oxygen-saturated and electron mediator-free PBS (pH = 4.4) recorded under the open circuit potential of 100 mV was depicted in Fig. 14A. The photo-electrocatalytic activity was inactive when the external illumination was cut off. The photo-electrocatalytic current would be increased remarkably when the irradiation was restored to the open status. It should be noticed that the background photo-electrocatalytic current of ITO electrode on the basis of nano-complex alone was not close to zero for the presence of photo-sensitive element (i.e., TiO_2) [13]. The photo-electrocatalytic efficiency on ORR for Lac based electrode was improved slightly in comparison to that of nano-composite based ITO electrode. Such result was in accordance with the analysis in UV–Vis spectra as described early. Low current response to Lac-induced catalysis on ORR should be blamed for inferior dynamics of heterogeneous charge convection, subsequent recognition and transformation of substrate as discussed previously. This result also implied that the combination of Lac with P25 would not enhance the active energy in the process of charge-hole abruption and charge shuttle from valence band to conductive one seriously.

Dependence curves of incident photon to current conversion efficiency (IPCE) on sweeping wavelength for both electrodes: P25-GO nano-composite alone based electrode and Lac/P25-GO-CTS/ITO were exhibited in Fig. 14B. IPCE could be calculated with the similar means introduced elsewhere [13]. It was obvious that IPCE of Lac based electrode was slightly improved in comparison to that of electrode on the basis of nano-complex alone within the whole range of scanning wavelength. This result convinced that the coordination between Lac and P25 would contribute to the elevation in charge transportation and utilization performance of external illumination. Such ligation would cut down the active energy of photo-induced electron transportation. It was in compliance with the analysis in UV–Vis spectra mentioned early.

4. Conclusion

P25 in combination with GO via covalent linkage was employed herein as a host platform to accommodate Lac molecules in virtue of chemical coupling and adjoining complexation. Efforts were made to investigate the influence of mutual interactions between component of P25-GO nano-complex and Lac immobilization on physiochemical features of nano-composite with Lac accommodation as well as kinetics of Lac-involved catalysis on ORR. Results from characterizations, tests and evaluations implied that synergistic effect of mutual interactions between elements of nano-composite and Lac molecules would render random array of enzyme molecules on the surface of supporting matrix. Such interactions would not impose seriously negative effect on photo-electrochemical activity of nano-complex itself and would lead to the improved hydrophilicity from the introduction of abundant hydrophilic groups on the outer surface of nano-complex. The process of dissolved oxygen molecule diffusion should be imputed to the key step in restraining the catalytic efficiency in electro-reduction of O_2 for P25-GO nano-complex with Lac attachment. Abutting ligation between P25 and Lac could contribute to the improvement in utilization of external irradiation to some extent. Main achievment in this work in comparison to those previous research efforts could be summarzied as follows:1). The synergy of covalent bonding and adjacent coordination between Hb and P25 would produce novel intermediate with distinct spectral character and electro-chemical behavior. Such combination would lead to the suppression in the efficiency of charge transferring of cofactor in Lac and redox site within P25 would play the role of primary active site in nano-complex with Lac integration; 2). The adjoining complexation between Lac and P25 would not exercise its catalytic activity towards ORR of Lac integration into nano-composite fully with elevated active energy; 3). Direct contact of metal element in nano-complex with enzyme molecule would impose considerable effect on the heterogeneous process and substrate-recognition and subsequent transformation steps. Intensity of

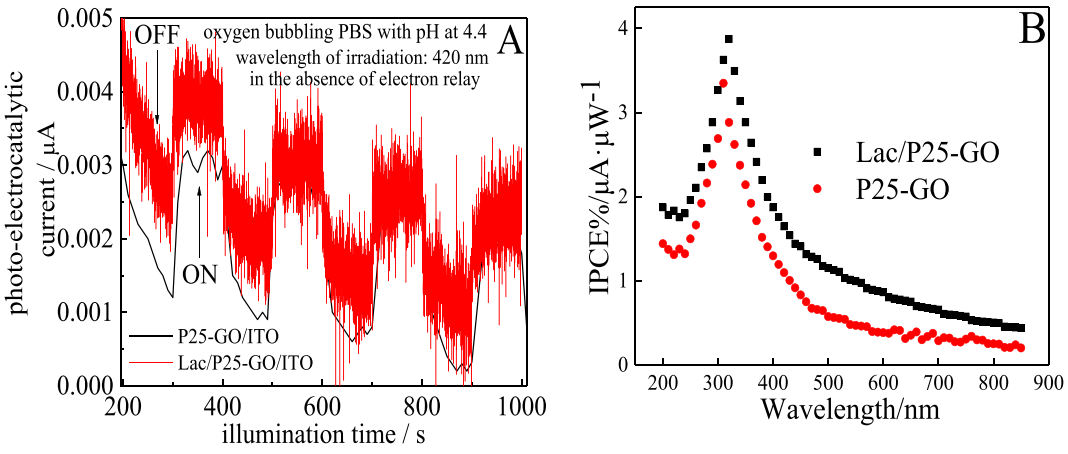

Fig. 14. Relationship curve of photo-electrocatalytic activity versus illumination time for immobile Lac based electrode in charge relay-free PBS (pH = 4.4) saturated by dissolved oxygen gas registered under the open circuit potential of 100 mV and irradiation wavelength at 420 nm, status of light path switching between "on" and "off" at different time intervals (A); dependence curves of IPCE on wavelength of incident irradiation for electrode on the basis of P25-GO nano-complex alone and Lac/P25-GO-CTS/ITO in oxygen-saturated PBS (pH = 4.4) recorded at the open circuit potential of 0.1 V.

influence could be dominated by the strength of abutting ligation which could be decided by the metal atoms in nano-complex and the specific amino acid groups on the surface or near to active site of redox protein molecules.

Declaration of Competing Interest

The authors declare that they have no known competing financial interests or personal relationships that could have appeared to influence the work reported in this paper.

Acknowledgements

The project was financially subsidized by the Xin-Jiang autonomous region colleges and universities scientific research plan-key projects of natural science (XJEDU2021I020) and the "13th five-year" plan for key discipline chemistry, Xinjiang normal university.

References

[1] F. Fischer, Photoelectrode, photovoltaic and photosynthetic microbial fuel cells, Renew. Sust. Energ. Rev. 90 (2018) 16–27, https://doi.org/10.1016/j.rser.2018.03.053.

[2] S. Ali, M.C. Flores, A. Razzaq, S. Sorcar, C.B. Hiragond, H.R. Kim, Y.H. Park, Y. Hwang, H.S. Kim, H. Kim, E.H. Gong, J. Lee, D. Kim, S.I. In, Gas phase photocatalytic CO2 reduction, "a brief overview for benchmarking", Catalysts. 9 (9) (2019) 727, https://doi.org/10.3390/catal9090727.

[3] Q. Zhang, Q.X. Hou, G.X. Huang, Q. Fan, Removal of heavy metals in aquatic environment by graphene oxide composites: a review, Environ. Sci. Pollut. R. 27 (1) (2020) 190–209, https://doi.org/10.1007/s11356-019-06683-w.

[4] Y. Huang, J. Li, Y.X. Yang, H.M. Yuan, Q.M. Wei, X.N. Liu, Y. Zhao, C.Y. Ni, Characterization of enzyme-immobilized catalytic support and its exploitation for the degradation of methoxychlor in simulated polluted soils, Environ. Sci. Pollut. R. 26 (27) (2019) 28328–28340, https://doi.org/10.1007/s11356-019-05937-x.

[5] B.C. Hernández-Majalca, M.J. Meléndez-Zaragoza, J.M. Salinas-Gutiérrez, A. Lopez-Ortiz, V. Collins-Martínez, Visible-light photo-assisted synthesis of GO-TiO_2 composites for the photocatalytic hydrogen production, Int. J. Hydrog. Energy. 44 (24) (2019) 12381–12389, https://doi.org/10.1016/j.ijhydene.2018.10.152.

[6] E. Kusiak-Nejman, A.W. Morawski, TiO_2/graphene-based nanocomposites for water treatment: a brief overview of charge carrier transfer, antimicrobial and photocatalytic performance, Appl. Catal. B. 253 (2019) 179–186, https://doi.org/10.1016/j.apcatb.2019.04.055.

[7] H.M. Albishri, D.A. El-Hady, Hyphenation of enzyme/graphene oxide-ionic liquid/glassy carbon biosensors with anodic differential pulse stripping voltammetry for reliable determination of choline and acetylcholine in human serum, Talanta 200 (2019) 107–114, https://doi.org/10.1016/j.talanta.2019.03.028.

[8] R. Tarasi, M. Alipour, L. Gorgannezhad, S. Imanparast, A. Yousefi-Ahmadipour, A. Ramezani, M.R. Ganjali, A. Shaflee, M.A. Faramarzi, M. Khoobi, Laccase immobilization onto magnetic β-cyclodextrin-modified chitosan: improved enzyme stability and efficient performance for phenolic compounds elimination, Macromol. Res. 26 (8) (2018) 755–762, https://doi.org/10.1007/s13233-018-6095-z.

[9] W.S. Sun, S.R. Yu, J.W. Liu, Y. Ke, J. Sun, Highly sensitive and selective detection of glucose by electrochemical sensor based on mesoporous silica coated graphene oxide nanosheet, Int. J. Electrochem. Sc. 16 (2) (2021), https://doi.org/10.20964/2021.02.51.

[10] S. Xu, Y. Liu, W. Zhao, Q. Wu, Y. Chen, X. Huang, Z. Sun, Y.e. Zhu, X. Liu, Hierarchical 0D–2D bio-composite film based on enzyme-loaded polymeric nanoparticles decorating graphene nanosheets as a high-performance bio-sensing platform, Biosens. Bioelectron. 156 (2020) 112134, https://doi.org/10.1016/j.bios.2020.112134.

[11] Y. Chen, X.Z. Meng, H.W. Gu, H.C. Yi, W.Y. Sun, A dual-response biosensor for electrochemical and glucometer detection of DNA methyltransferase activity based on functionalized metal-organic framework amplification, Biosens. Bioelectron. 134 (2019) 117–122, https://doi.org/10.1016/j.bios.2019.03.051.

[12] A.G. Jacob, R.A. Wahab, N.A. Mahat, Ternary biogenic silica/magnetite/graphene oxide composite for the hyperactivation of Candida rugosa lipase in the esterification production of ethyl valerate, Enzyme. Microb. Tech. 148 (2021) 109807, https://doi.org/10.1016/j.enzmictec.2021.109807.

[13] S.C. Wang, J.S. Cai, J.J. Mao, S.H. Li, J.L. Shen, S.W. Gao, J.Y. Huang, X.Q. Wang, P.P. Ivan, Y.K. Lai, Defective black Ti3+ self-doped TiO_2 and reduced graphene oxide composite nanoparticles for boosting visible-light driven photocatalytic and photoelectrochemical activity, Appl. Surf. Sci. 467–468 (2019) 45–55, https://doi.org/10.1016/j.apsusc.2018.10.138.

[14] H. Wu, B.J. Sun, D.Q. Huang, Y.T. Liu, H. Zhang, Characterization, direct electrochemistry, and electrocatalysis of immobilized hemoglobin on a platinum nanoparticle−didodecyldimethylammonium bromide composite film, Anal. Lett. 49 (4) (2016) 556–567, https://doi.org/10.1080/00032719.2015.1075133.

[15] H.Y. Zhao, H.M. Zhou, J.X. Zhang, W. Zheng, Y.F. Zheng, Carbon nanotube–hydroxyapatite nanocomposite: a novel platform for glucose/O_2 biofuel cell, Biosens. Bioelectron. 25 (2) (2009) 463–468, https://doi.org/10.1016/j.bios.2009.08.005.

[16] M. Zhang, M. Zhang, S.W. Zhang, H. Zeng, Direct electrochemistry and photoelectro-catalysis on oxygen reduction reaction of titanium dioxide nano-tubes sensitized by Meso-Tetrakis (4-carboxyphenyl) porphine with laccase accommodation, Macromol. Res. 29 (1) (2021) 62–74, https://doi.org/10.1007/s13233-021-9008-5.

[17] M.i. Zhang, Y.-H. Zhang, T.-M. Ma, H. Zeng, Comparison in electro-catalytic function to reduction of hydrogen peroxide for two nano-structure electrodes with myoglobin immobilization, Chem. Phys. Lett. 738 (2020) 136904, https://doi.org/10.1016/j.cplett.2019.136904.

[18] J. Huang, J.Y. Zhou, H.Y. Xiao, S.Y. Long, J.T. Wang, Study of CuTAPC-Fe_3O_4 Nanoparticles and their laccase immobilization, Acta. Chim. Sinica. 63 (14) (2005) 1343–1347. (in Chinese) https://doi.org/10.3321/j.issn:0567-7351.2005.14.017.

[19] Y. Yang, W.S. Huo, Z. Zhou, Q. Zhang, H. Zeng, Direct Electrochemistry of Electrode Modified with Thin Film of laccase Immobilized in Nano-Composite of Polyaniline-CoC2O4, Chin. J. Inorg. Chem. 32 (12) (2016) 2117-2128. (in Chinese) https://doi.org/10.11862/CJIC.2016.277.

[20] H.J. Qiu, C.X. Xu, X.R. Huang, Y. Ding, Y.B. Qu, P.J. Gao, Immobilization of laccase on nanoporous gold: comparative studies on the immobilization strategies and the particle size effects, J. Phys. Chem. C. 113 (6) (2009) 2521–2525, https://doi.org/10.1021/jp8090304.

[21] Y.L. Wang, Z.C. Wang, Y.P. Rui, M.G. Li, Horseradish peroxidase immobilization on carbon nanodots/CoFe layered double hydroxides: direct electrochemistry and hydrogen peroxide sensing, Biosens. Bioelectron. 64 (2015) 57–62, https://doi.org/10.1016/j.bios.2014.08.054.

[22] X.Q. Chu, M. Zhang, W.S. Huo, H. Zeng, Y. Yang, 2-hydroxy-4-amino-azobenzene modified graphene oxide with incorporation of bilirubin oxidase for

photoelectrochemical catalysis of oxygen reduction reaction, Int. J. Electrochem. Sc. 15 (2020) 11531–11554, https://doi.org/10.20964/2020.11.46.
[23] T.-F. Yeh, J.-M. Syu, C. Cheng, T.-H. Chang, H. Teng, Graphite oxide as a photocatalyst for hydrogen production from water, Adv. Funct. Mater. 20 (14) (2010) 2255–2262, https://doi.org/10.1002/adfm.v20:1410.1002/adfm.201000274.
[24] X.Y. He, D.J. Ren, Z.Q. Deng, H. Liu, S.Q. Zhang, X.Q. Zhang, Effect of additives on acid-base stability of laccase and its protective mechanism, Food. Ferment. Ind. 43 (12) (2017) 20-24. (in Chinese) https://doi.org/10.13995/j.cnki.11-1802/ts.015196.
[25] H. Mao, B.F. Cai, B. Zhao, Z.W. Wang, Molecular simulation and spectroscopic studies of interactions between sultan red II and myoglobin, Chin. J. Appl. Chem. 11 (2009) 1332–1335, https://doi.org/10.3969/j.issn.1000-0518.2009.11.018 (in Chinese).
[26] M. Du, J. Zhang, M. Chou, Inhibition Mechanism of Imidazoline Derivative Inhibitor for Q235 Steel in Saltwater Saturated with CO2, Acta. Phys.-Chim. Sin. 24 (01) (2008) 138-142. (in Chinese) https://doi.org/10.3866/PKU.WHXB20080124.
[27] S.G. Hong, J.H. Kim, R.E. Kim, S.J. Kwon, D.W. Kim, H.T. Jung, J.S. Dordick, J. Kim, Immobilization of glucose oxidase on graphene oxide for highly sensitive biosensors, Biotechnol. Bioproc. E. 21 (4) (2016) 573–579, https://doi.org/10.1007/s12257-016-0373-4.
[28] S. Shleev, J. Tkac, A. Christenson, T. Ruzgas, A.I. Yaropolov, J.W. Whittaker, L. Gorton, Direct electron transfer between copper-containing proteins and electrodes, Biosens. Bioelectron. 20 (12) (2005) 2517–2554, https://doi.org/10.1016/j.bios.2004.10.003.
[29] H.P. Peng, R.P. Liang, L. Zhang, J.D. Qiu, Facile preparation of novel core-shell enzyme-Au-polydopamine-Fe_3O_4 magnetic bionanoparticles for glucose sensor, Biosens. Bioelectron. 42 (2013) 293–299, https://doi.org/10.1016/j.bios.2012.10.074.
[30] M.A. Rahman, H.B. Noh, Y.B. Shim, Direct electrochemistry of laccase immobilized on Au nanoparticles encapsulated-dendrimer bonded conducting polymer: application for a catechin sensor, Anal. Chem. 80 (21) (2008) 8020–8027, https://doi.org/10.1021/ac801033s.
[31] H.J. Qiu, C.X. Xu, X.R. Huang, Y. Ding, Y.B. Qu, P.J. Gao, Adsorption of laccase on the surface of nanoporous gold and the direct electron transfer between them, J. Phys. Chem. C. 112 (38) (2008) 14781–14785, https://doi.org/10.1021/jp805600k.
[32] S. Cosnier, A.J. Gross, A.L. Goff, M. Holzinger, Recent advances on enzymatic glucose/oxygen and hydrogen/oxygen biofuel cells: achievements and limitations, J. Power. Source. 325 (2016) 252–263, https://doi.org/10.1016/j.jpowsour.2016.05.133.
[33] S. Tsujimura, Y. Kamitaka, K. Kano, Diffusion-controlled oxygen reduction on multi-copper oxidase-adsorbed carbon aerogel electrodes without mediator, Fuel. Cells. 7 (6) (2007) 463–469, https://doi.org/10.1002/fuce.200700032.
[34] W.E. Farneth, B.A. Diner, T.D. Gierke, M.B. D'Amore, Current densities from electrocatalytic oxygen reduction in laccase/ABTS solutions, J. Electroanal. Chem. 581 (2) (2005) 190–196, https://doi.org/10.1016/j.jelechem.2005.03.025.
[35] N. Mano, H.H. Kim, Y.C. Zhang, A. Heller, An oxygen cathode operating in a physiological solution, J. Am. Chem. Soc. 124 (22) (2002) 6480–6486, https://doi.org/10.1021/ja025874v.
[36] Y. Amano, A. Koto, S. Matsuzaki, H. Sakamoto, T. Satomura, S.-I. Suye, Construction of a biointerface on a carbon nanotube surface for effificient electron transfer, Mater. Lett. 174 (2016) 184–187, https://doi.org/10.1016/j.matlet.2016.03.113.